Eur. Phys. J. D **14**, 337–348 (2001)

THE EUROPEAN PHYSICAL JOURNAL D

EDP Sciences
© Società Italiana di Fisica
Springer-Verlag 2001

Simulation of the ignition transient in RF inductively-coupled plasma torches

D. Bernardi[1], V. Colombo[2,a], G.G.M. Coppa[1,b], and A. D'Angola[1]

[1] Istituto Nazionale per la Fisica della Materia and Dipartimento di Energetica, Politecnico di Torino, Corso Duca degli Abruzzi 24, 10129 Torino, Italy
[2] Università degli Studi di Bologna, Dipartimento di Ingegneria delle Costruzioni Meccaniche, Nucleari, Aeronautiche e di Metallurgia and C.I.R.A.M., Via Saragozza 8, 40123 Bologna, Italy

Received 29 December 2000

Abstract. The paper deals with the time-dependent numerical simulation of inductively-coupled plasma torches during the ignition transient, which is induced by a graphite rod and leads to the final, self-sustaining plasma condition. The study has been performed by using a 2D time-dependent fluid-magnetic code based on the SIMPLER algorithm within the assumptions of laminar flow, local thermodynamic equilibrium conditions and optically thin plasma. The graphite rod has been treated as a real obstacle for the gas and the electron emission due to the thermoionic effect has been suitably taken into account. The advantage of using a time-dependent code in order to select different plasma operating conditions that can lead to stable discharges is pointed out. Results for both argon and air discharges are presented for different torch geometries, RF frequencies and inlet gas configurations (also including the presence of a carrier gas injected along the axis of the torch). Moreover, the final self-sustaining plasma configurations obtained are compared, when available, with results coming from static models, which have been published by other authors.

PACS. 52.75.Hn Plasma torches – 52.65.-y Plasma simulation – 52.80.Pi High-frequency and RF discharges

1 Introduction

The behaviour of inductively-coupled plasma torches is usually studied by static models [1,4], which are capable of predicting plasma temperature, velocity and electromagnetic field distributions for steady, self-sustaining plasma configurations. In such models, the system of non-linear equations governing the temperature and velocity fields of the ionized gas and the electromagnetic field is typically solved by means of iterative techniques. In this frame, the initial electric conductivity of the gas is taken high enough so that the heat generation due to the induction currents does not vanish.

However, in some cases, a code based upon static models may not converge because of numerical instabilities, although the stationary, self-sustaining plasma configuration for the selected operating parameters is experimentally proved to exist. In fact, as static models do not allow the numerical procedure to follow the real dynamic evolution of the system, the possibility of passing through non-physical configurations for the plasma during the iterations cannot be avoided. Such a drawback may have a relevant impact in the design of a torch system, as one cannot decide whether a failure in the convergence of the numerical process has to be ascribed to computational instabilities or, rather, to the physical non-sustainability of the discharge for the selected operating parameters.

In order to overcome such a difficulty and with the aim of obtaining a helpful tool for optimizing the design procedures, a fully two dimensional (r, z) time-dependent code has been developed. The code is able to perform the analysis of the dynamic behaviour of the torch during the ignition transient which leads to the self-sustaining condition for the plasma. The plasma initiation technique considered in this work makes use of a graphite rod initially inserted in the coil region and then gradually extracted. The presence of the rod, which is heated by the RF field, causes a local increase in the electric conductivity of the cold, non-ionized gas by thermoionic effect, so inducing the plasma ignition. The rod has been simulated as a real obstacle for the fluid and its radiation emission has been supposed negligible. The thermoionic effect has been treated in a consistent manner with respect to the rod surface temperature (namely, the increase in the gas electric conductivity near the rod has been related to the graphite surface temperature coming from the solution of the energy equation). Moreover, the possibility of taking

[a] e-mail: colombo@ciram.ing.unibo.it
[b] e-mail: ggmcoppa@polito.it

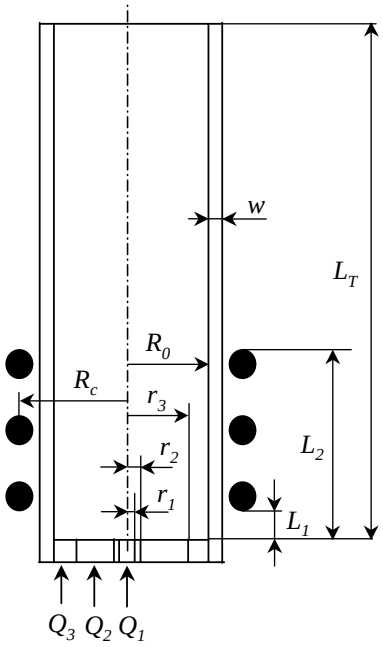

argon	air
$r_1 = 1.7$ mm	$r_1 = 0$ mm
$r_2 = 3.7$ mm	$r_2 = 0$ mm
$r_3 = 18.8$ mm	$r_3 = 18.8$ mm
$R_0 = 25$ mm	$R_0 = 30$ mm
$R_c = 33$ mm	$R_c = 38$ mm
$L_1 = 10$ mm	$L_1 = 30$ mm
$L_2 = 74$ mm	$L_2 = 94$ mm
$L_T = 250$ mm	$L_T = 200$ mm
$w = 2$ mm	$w = 2$ mm

Fig. 1. Scheme of the plasma torch.

into account the presence of a carrier gas injected along the axis of the torch has been included in the code.

Several simulations have been performed using both argon (Sect. 4.1) and air (Sect. 4.2) as plasma gas and results are presented including some test cases concerning the final self-sustaining plasma conditions.

2 Physical model

The typical torch geometry considered in the present work is shown in Figure 1. The physical model of the torch is based upon the following basic assumptions [3]:

- axisymmetric geometry,
- optically thin plasma,
- local thermodynamic equilibrium conditions for the ionized gas,
- laminar flow,
- gas velocity does not have tangential component,
- negligible viscous dissipation and pressure work,
- negligible displacement current and electrostatic fields,
- Ohm's law is expressed simply as $\mathbf{J} = \sigma\mathbf{E}$, assuming negligible the effect of the magnetic field.

The model includes the continuity equation for the gas density, ρ:

$$\frac{\partial \rho}{\partial t} + \frac{1}{r}\frac{\partial}{\partial r}\left(r\rho v_r\right) + \frac{\partial}{\partial z}\left(\rho v_z\right) = 0 \tag{1}$$

the Navier-Stokes equations for the radial and axial components of the velocity, v_r and v_z:

$$\rho\left(\frac{\partial v_r}{\partial t} + v_r\frac{\partial v_r}{\partial r} + v_z\frac{\partial v_r}{\partial z}\right) = -\frac{\partial p}{\partial r} - \frac{2\mu v_r}{r^2} + \frac{2}{r}\frac{\partial}{\partial r}\left(\mu r\frac{\partial v_r}{\partial r}\right) + \frac{\partial}{\partial z}\left[\mu\left(\frac{\partial v_r}{\partial z} + \frac{\partial v_z}{\partial r}\right)\right] + F_r \tag{2}$$

$$\rho\left(\frac{\partial v_z}{\partial t} + v_r\frac{\partial v_z}{\partial r} + v_z\frac{\partial v_z}{\partial z}\right) = -\frac{\partial p}{\partial z} + 2\frac{\partial}{\partial z}\left(\mu\frac{\partial v_z}{\partial z}\right) + \frac{1}{r}\frac{\partial}{\partial r}\left[r\mu\left(\frac{\partial v_z}{\partial r} + \frac{\partial v_r}{\partial z}\right)\right] + F_z \tag{3}$$

and the conduction-convection equation for the temperature field, T:

$$\rho c_{\mathrm{p}}\left(\frac{\partial T}{\partial t} + v_r\frac{\partial T}{\partial r} + v_z\frac{\partial T}{\partial z}\right) = \frac{1}{r}\frac{\partial}{\partial r}\left(rk\frac{\partial T}{\partial r}\right) + \frac{\partial}{\partial z}\left(k\frac{\partial T}{\partial z}\right) + Q - R \tag{4}$$

where F_r, F_z, Q and R are the radial and axial components of the Lorentz force, the Joule heating rate and the plasma radiation losses, respectively. The radiation emission from the graphite rod and the radiative heat exchange between the plasma and the rod have been supposed to be negligible.

To study the electromagnetic field generated by the coil and by the induction currents, a two-dimensional approach, similar to that described in reference [5], has been employed, in which the electric field, instead of the vector potential [6], has been chosen as main variable. This approach is described in detail here, as it differs from the ones usually employed [3,4]. Under the assumptions listed above, the Maxwell equations reduce to:

$$\nabla \times \mathbf{B} = \mu_0\left(\sigma\mathbf{E} + \mathbf{j}^{(\mathrm{coil})}\right) \tag{5}$$

$$\nabla \times \mathbf{E} = -\frac{\partial \mathbf{B}}{\partial t} \tag{6}$$

where the electric and magnetic fields

$$\mathbf{E} = \mathbf{e}_\theta E_\theta(r,z)\mathrm{e}^{\mathrm{i}\omega t}$$
$$\mathbf{B} = \mathbf{e}_r B_r(r,z)\mathrm{e}^{\mathrm{i}\omega t} + \mathbf{e}_z B_z(r,z)\mathrm{e}^{\mathrm{i}\omega t}$$

and the coil current density

$$\mathbf{j}^{(\mathrm{coil})} = \mathbf{e}_\theta j_\theta \mathrm{e}^{\mathrm{i}\omega t}$$

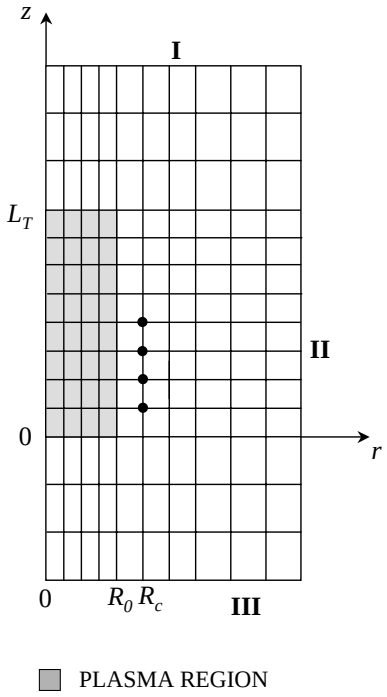

Fig. 2. Sketch of the computational domain. The symbols I, II and III denote the borders of the domain for the calculation of the electromagnetic field.

are supposed to be sinusoidal with the frequency $f = \omega/2\pi$. By casting equations (5, 6) in cylindrical coordinates, one obtains:

$$\frac{1}{r}\frac{\partial}{\partial r}\left(r\frac{\partial E_\theta}{\partial r}\right) - \frac{E_\theta}{r^2} + \frac{\partial^2 E_\theta}{\partial z^2} = \mathrm{i}\omega\mu_0\left(\sigma E_\theta + j_\theta\right) \tag{7}$$

$$B_r = \frac{1}{\mathrm{i}\omega}\frac{\partial E_\theta}{\partial z}, \quad B_z = -\frac{1}{\mathrm{i}\omega}\frac{1}{r}\frac{\partial}{\partial r}\left(rE_\theta\right). \tag{8}$$

These equations are coupled to equations (1–4) through the radial and axial components of the Lorentz force and through the Joule heating rate:

$$F_r = \frac{1}{2}\sigma\left(T\right)\mathrm{Re}\left[E_\theta B_z^*\right], \tag{9}$$

$$F_z = -\frac{1}{2}\sigma\left(T\right)\mathrm{Re}\left[E_\theta B_r^*\right], \tag{10}$$

$$Q = \frac{1}{2}\sigma\left(T\right)\left|E_\theta\right|^2. \tag{11}$$

Equation (7) for the electric field, E_θ, has been spatially discretized by a finite-difference technique over a non-uniform grid covering a computational domain bigger than the torch region (Fig. 2). The current density, j_θ, in the equation (7), has been set to zero everywhere except that at the grid points located in the coil region ($r = R_c$). The borders of the domain, denoted by I, II and III in Figure 2, have been placed far enough from the plasma region in order to use boundary conditions for the electric field as if the torch were a magnetic dipole produced by the electric current flowing in the plasma and in the induction coil. The electric field generated by a time-harmonic magnetic dipole shows the spatial behaviour:

$$E_\theta = \frac{Ar}{\left(r^2 + z^2\right)^{\frac{3}{2}}} \tag{12}$$

being the dipole located in the origin of the cylindrical (r, z) coordinates having the z-axis parallel to the dipole. By taking the r-derivative of the equation (12) and eliminating the unknown constant, A, one obtains a boundary condition to be applied on the lateral border (II) of the domain:

$$\frac{\partial E_\theta}{\partial r} = \frac{\left[1 - 3r^2\left(r^2 + z^2\right)^{-1}\right]}{r}E_\theta. \tag{13}$$

In the same manner, by taking the z-derivative of equation (12), the following boundary condition is obtained for the upper (I) and the lower (III) borders:

$$\frac{\partial E_\theta}{\partial z} = -\frac{3z}{r^2 + z^2}E_\theta. \tag{14}$$

On the axis of the torch ($r = 0$), the symmetry condition, $E_\theta = 0$, has been imposed.

The boundary conditions for the velocity and the temperature fields are summarized below (see Figs. 1 and 2).

– *Inlet* ($z = 0$):

$$v_r = 0$$

$$v_z = \begin{cases} Q_1/\left(\pi r_1^2\right) & r < r_1 \\ 0 & r_1 \le r \le r_2 \\ Q_2/\left[\pi\left(r_3^2 - r_2^2\right)\right] & r_2 < r \le r_3 \\ Q_3/\left[\pi\left(R_0^2 - r_3^2\right)\right] & r_3 < r < R_0 \end{cases}$$

$$T = T_{\mathrm{in}}.$$

– *Axis* ($r = 0$):

$$v_r = 0, \ \frac{\partial v_z}{\partial r} = 0, \ \frac{\partial T}{\partial r} = 0.$$

– *Wall* ($r = R_0$):

$$v_r = v_z = 0, \ -k\frac{\partial T}{\partial r} = \frac{k_w}{w}\left(T - T_w\right)$$

where k_w and T_w are the thermal conductivity and the external temperature of the confinement tube, respectively.

– *Exit* ($z = L_{\mathrm{T}}$): rigorous conditions for the outflow boundary cannot be expressed in a simple way. However, when the post-coil region is long enough, heat convection usually prevails over conduction at the exit of the torch (*i.e.*, the Peclet number is large). In this case, typical one-way conditions [7] can be applied:

$$\frac{\partial v_r}{\partial z} = 0, \ \frac{\partial\left(\varrho v_z\right)}{\partial z} = 0, \ \frac{\partial T}{\partial z} = 0.$$

When the graphite rod is inserted in the torch, the following additional boundary conditions must be specified on the rod borders (refer to Fig. 3).

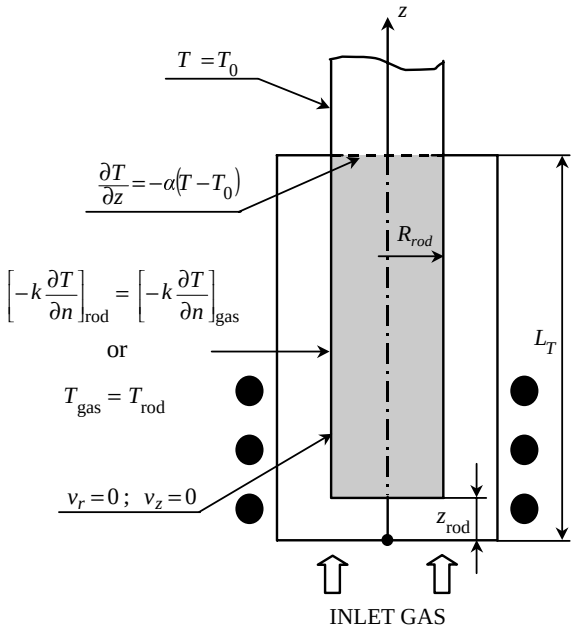

Fig. 3. Boundary conditions on the rod borders.

– *Plasma-graphite interfaces* ($r = R_{\rm rod}$; $z \geq z_{\rm rod}$ and $r \leq R_{\rm rod}$; $z = z_{\rm rod}$):

$$v_r = v_z = 0$$
$$\left[-k\frac{\partial T}{\partial n}\right]_{\rm rod} = \left[-k\frac{\partial T}{\partial n}\right]_{\rm gas} \tag{15}$$

where n represents the normal direction to the rod surface, or, alternatively:

$$T_{\rm gas} = T_{\rm rod} \tag{16}$$

where $T_{\rm rod}$ is a fixed, prescribed value for the rod temperature assumed as uniform. Both options (15) and (16) have been included in the numerical code. When (15) is used, the self-consistent temperature field is calculated all over the torch domain, including the region occupied by the graphite rod. On the contrary, when (16) is chosen, the energy equation (4) is solved over the plasma region only, while the rod temperature is supposed to be maintained at a space-uniform, time-constant value. In the former case, further boundary conditions are necessary on the remaining borders of the rod.

– *Rod axis* ($r = 0$; $z \geq z_{\rm rod}$):

$$\frac{\partial T}{\partial r} = 0.$$

– *Rod border at torch exit* ($z = L_{\rm T}$; $r \leq R_{\rm rod}$): in the region occupied by the rod, the only heat transfer mechanism involved is the conduction across the graphite. Consequently, on the rod border located at the exit of the torch, a completely different condition for T must be imposed. To this purpose, the rod has been treated as infinitely long in the axial direction outside the torch. This allows one to obtain a boundary condition that relates the graphite temperature to its axial derivative. In fact, the energy equation governing the heat transfer in the part of the rod extending outside the torch can be written, by dropping the time-derivative term, as:

$$\frac{\partial^2 T}{\partial r^2} + \frac{1}{r}\frac{\partial T}{\partial r} + \frac{\partial^2 T}{\partial z^2} = 0 \tag{17}$$

by assuming that the characteristic time of variation of the temperature for the gas is much shorter than that for the rod. To solve this equation, a fixed value of the temperature, T_0, has been imposed on the rod surface. By separation of variables, the following solution for equation (17) can be found:

$$T(r,z) = BJ_0(\alpha r)\,{\rm e}^{-\alpha z} + T_0 \tag{18}$$

where J_0 denotes the zeroth order Bessel function of the first kind and $\alpha = j_{01}/R_{\rm rod}$. Finally, by taking the z-derivative of (18) one can eliminate the unknown constant, B, obtaining the relationship:

$$\frac{\partial T}{\partial z} = -\alpha\,(T - T_0)$$

which provides the boundary condition to be used on the rod border laying at the exit of the torch.

3 Numerical solution and ignition transient simulation

The system of equations (1–4, 7) has been spatially discretized by using a finite-volume method. A fully implicit Euler method has been employed for time discretization. The resulting non-linear algebraic equations are solved by means of an iterative procedure based on the SIMPLER algorithm [7]. At each time step, iterations are performed until a solution for the non-linear system of equations is found with the required precision. The calculations are performed until the steady state or the final time level is reached.

The ignition of the gas is induced by the thermoionic emission of the graphite rod heated by the RF field generated by the coil, which causes a consistent increase of the electric conductivity of the gas in a thin region surrounding the rod, making the gas capable of absorbing power from the electromagnetic field. The effect of the heating of the gas by the rod is negligible, as the gas reaches a sufficient electric conductivity at temperatures of $6 \div 7 \times 10^3$ K, well beyond the melting point of the graphite. When the gas has reached a temperature high enough to acquire a significant electric conductivity, it shields the rod from the electric field, preventing the graphite from achieving too high temperatures.

The simulation of the ignition transients studied in this work has been performed as follows: initially, the graphite rod is completely inserted in the torch, the power supply is supposed to be switched off and the non-ionized gas flows through the confinement tube at the temperature of 350 K. In this situation, only the Navier-Stokes

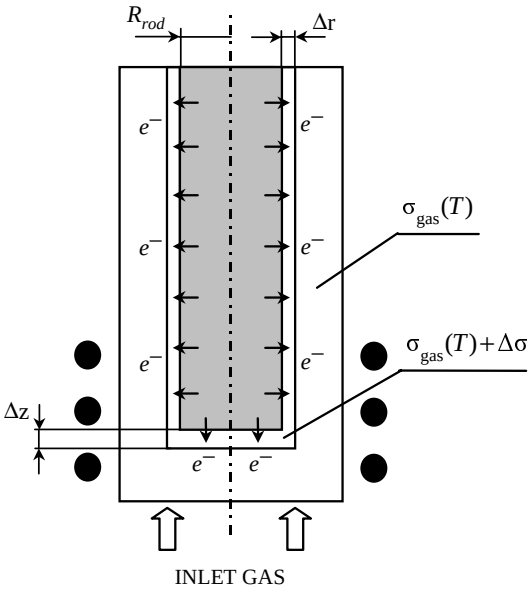

Fig. 4. Scheme of the torch with the modified-conductivity region near the rod. The values used in the simulations are: $R_{\rm rod}$ = 10 mm, Δr = 6 mm, Δz = 8 mm for argon and $R_{\rm rod}$ = 9 mm, Δr = 7.5 mm, Δz = 8 mm for air.

equations are to be solved. When the steady flow configuration is reached, the power generator is turned on and the solution of the whole set of equations is found. Then, the operating conditions are changed in time until the desired final values are achieved. The complex phenomena connected with the thermoionic emission have been simulated by considering a narrow region (whose radial and axial dimensions, Δr and Δz, are shown in Fig. 4) surrounding the rod, in which the electric conductivity of the gas has been calculated as:

$$\sigma = \sigma_{\rm gas}\,(T) + \Delta\sigma$$

where $\sigma_{\rm gas}\,(T)$ is the conductivity of the gas in absence of thermoionic effect while $\Delta\sigma$ is an additional term due to the electrons emitted by the graphite. The following relationship has been used for $\Delta\sigma$:

$$\Delta\sigma = \beta\,(T_{\rm s} - 350)$$

where $T_{\rm s}$ is the temperature of the rod surface and β is a suitable coefficient that makes the value of $\Delta\sigma$ high enough to allow the gas to absorb power from the electric field when $T_{\rm s} \simeq 10^3$ K. In this study, two values, 0.25 and 0.5 Ω^{-1} m^{-1} K^{-1}, have been considered for β.

The thermodynamic and transport properties of argon have been taken from reference [8], while updated values for the physical properties of air come from a recent work by Capitelli *et al.* [9]. The thermal and electric conductivities of graphite depend strongly upon the type of graphite being considered. In this study, physical data for the POCO AXF-5Q graphite have been used, assuming a mean constant value for the specific heat and the density.

4 Numerical results

4.1 Argon discharges

In order to test the reliability of the numerical procedure, calculations have been reproduced for some selected operating configurations taken from reference [2] by Boulos *et al.* The test cases concern an argon plasma torch working at atmospheric pressure and with a central injection of carrier gas. The torch geometry is sketched in Figure 1. The following operating conditions have been considered: discharge electric power P = 3 kW, generator frequency f = 3 MHz, plasma gas flow rate Q_2 = 3 slpm, total gas flow rate $Q_{\rm tot} = Q_1 + Q_2 + Q_3$ = 20 slpm. The mid-coil radial temperature and the axial velocity profiles of the plasma for the final, self-sustaining configurations corresponding to different values of the carrier gas flow rate, Q_1, are presented in Figure 5. For the same cases, Figure 6 shows the plasma temperature fields. In these simulations, the sheath gas flow rate, Q_3, has been varied in order to keep constant the total flow rate. The comparison of these results with those obtained by static codes reported in reference [2] shows that the temperature profiles are in very good agreement, while the velocities are lower with the time-dependent simulation, although the shape of the axial profiles is very similar. As demonstrated in reference [6], this is due to the one-dimensional approach used in reference [2] for the calculation of the electromagnetic field.

The use of a time-dependent numerical procedure has been proved to be very useful to overcome the numerical instabilities that static codes usually experience under high central injection conditions. In fact, time-dependent analyses give the possibility of gradually increasing the carrier gas flow rate during the transient or injecting it in the final stage of the initiation procedure, when the self-sustaining plasma is already established.

In order to highlight the effect of the various system operating parameters on the behaviour of the torch during the ignition transient, different types of initiation procedures have been considered. To study only the fluid-dynamic and thermal phenomena during the transient, without having to consider also the physical effects connected to the heat transport in the rod, some simulations have been performed by assuming a fixed value for the rod temperature. However, all these effects have been eventually taken into account in a consistent manner, by simulating a realistic ignition procedure, in which the temperature field in the rod has been obtained by the solution of the energy equation. All the calculations refer to the torch of Figure 1, working at atmospheric pressure without carrier gas ($Q_1 = 0$) and with f = 3 MHz, Q_2 = 3 slpm and Q_3 = 17 slpm.

A first type of transient has been simulated, in which the rod is completely inserted in the torch and its position is kept fixed, while the discharge electric power, P, is step-wise increased. The rod temperature, $T_{\rm rod}$, is fixed and a value of 0.5 Ω^{-1} m^{-1} K^{-1} for β is adopted. For each power level, the time-dependent calculation has been performed until the corresponding steady state was reached.

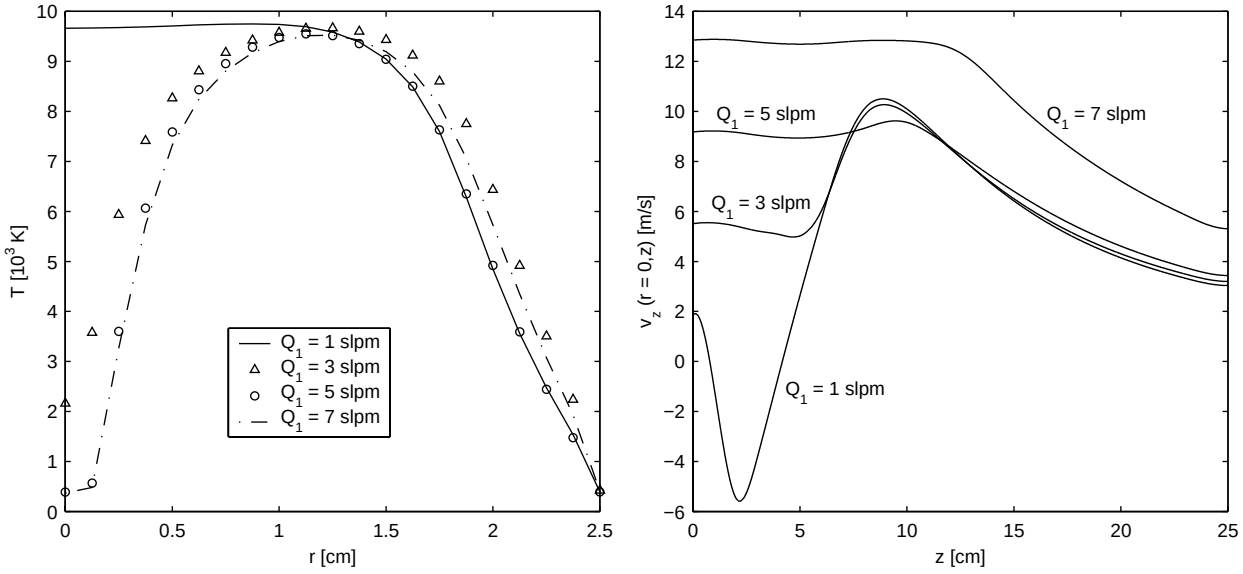

Fig. 5. Midcoil plasma temperature (left) and axial plasma velocity (right) profiles for self-sustaining argon discharges with different carrier gas flow rates.

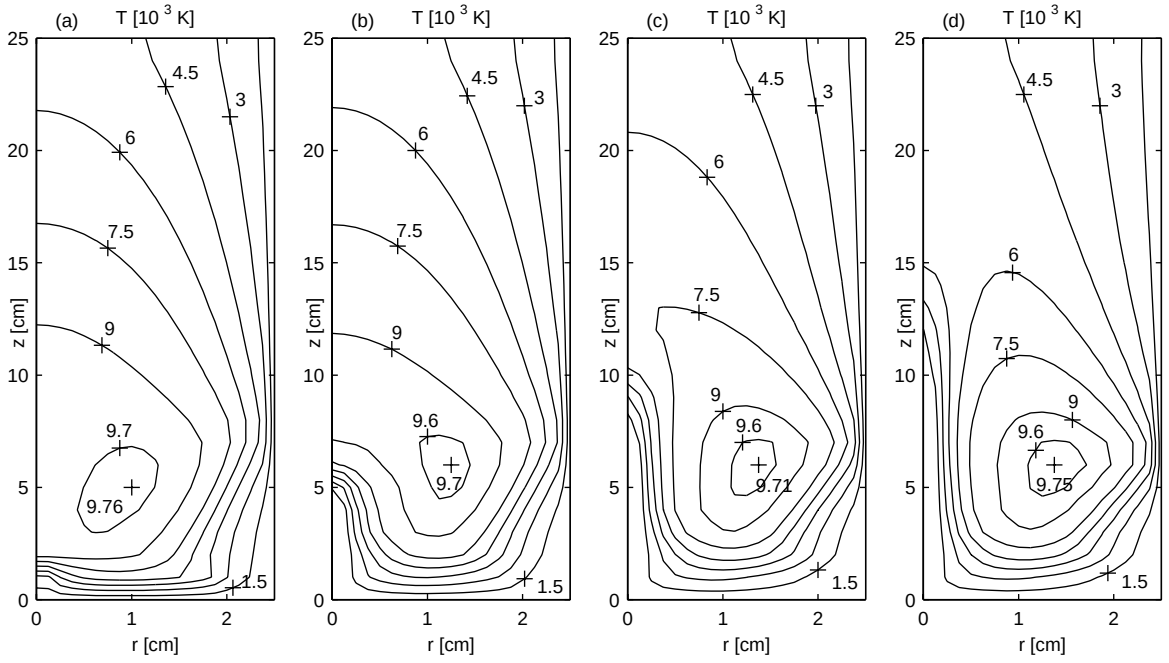

Fig. 6. Plasma temperature fields for the cases of Figure 5: (a) $Q_1 = 1$ slpm, (b) $Q_1 = 3$ slpm, (c) $Q_1 = 5$ slpm, (d) $Q_1 = 7$ slpm.

The operating conditions are fully detailed in Table 1, along with the corresponding discharge properties including the current per unit height of coil, I_{coil} (defined as NI_0/H, being N the number of coil turns, I_0 the current in each turn and $H = L_2 - L_1$ the height of the coil), the maximum plasma temperature, T_{max}, and the fraction of total input power, $\Delta P/P$, dissipated in the modified-conductivity region near the rod. The plasma temperature fields for some values of P are shown in Figure 7. The effect of the additional conductivity, $\Delta\sigma$, is highlighted in Table 2, where T_{m} is the maximum plasma temperature at midcoil and T_{m}^{*} represents the temperature of the gas

Table 1. Operating conditions and discharge properties for an argon ignition transient with fixed rod position and variable discharge power.

P [kW]	T_{rod} [K]	z_{rod} [mm]	I_{coil} [A/cm]	T_{max} [K]	$\Delta P/P$ [%]
1	2000	10	41.1	4850	88.5
1.5	2000	10	49.6	6190	88.5
2	2000	10	53.4	7590	86.0
2.5	2000	10	54.6	8510	76.7
3	2000	10	55.9	9030	65.8

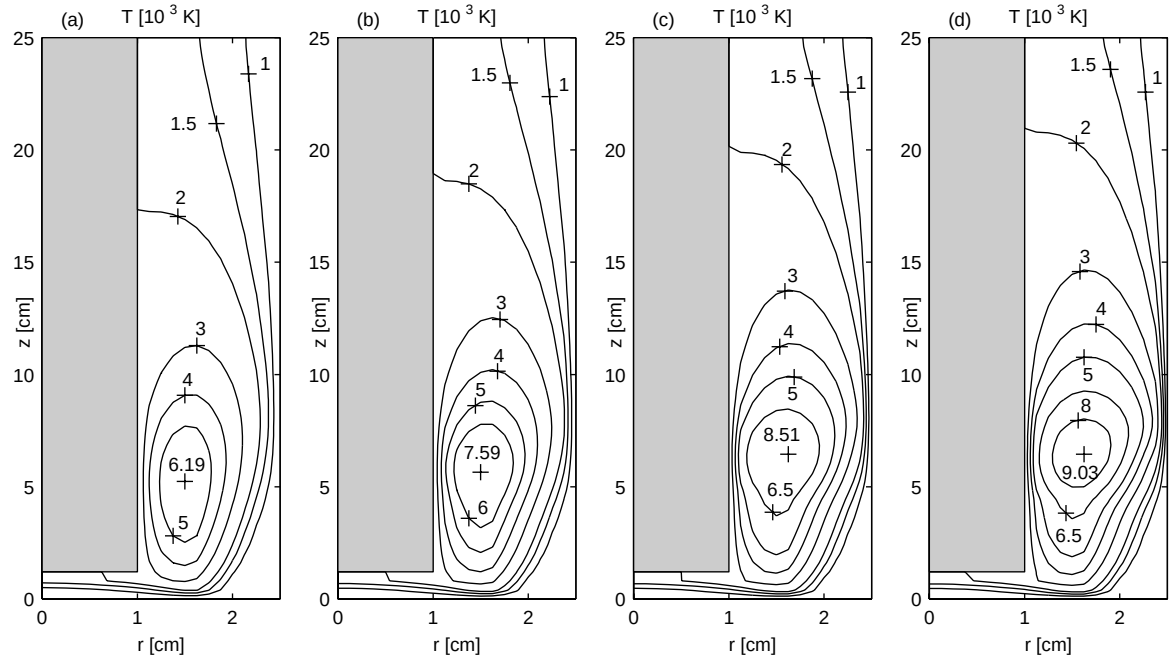

Fig. 7. Plasma temperature fields for the argon ignition transient described in Table 1: (a) $P = 1.5$ kW, (b) $P = 2$ kW, (c) $P = 2.5$ kW, (d) $P = 3$ kW.

Table 2. Effect of the parameter $\Delta\sigma$ on the plasma temperature for the cases of Table 1.

P [kW]	T_m [K]	$\sigma(T_\mathrm{m})$ [Ω^{-1} m^{-1}]	$\sigma(T_\mathrm{m}) + \Delta\sigma$ [Ω^{-1} m^{-1}]	T_m^* [K]
1	4700	4.2	829.2	7850
1.5	5930	64.5	889.5	7920
2	6640	196.2	1021.2	8100
2.5	6730	221.2	1046.2	8140
3	6840	259.0	1084.0	8200

Table 3. Operating conditions and discharge properties for an argon ignition transient with fixed discharge power and variable rod position.

P [kW]	T_rod [K]	z_rod [mm]	I_coil [A/cm]	T_max [K]	$\Delta P/P$ [%]
$\beta = 0.25$					
3	2000	20	67.1	9240	62.4
3	2000	30	50.7	9480	45.0
3	2000	50	46.6	9700	22.0
3	2000	74	47.6	9730	5.5
3	2000	150	47.7	9740	0.02
3	2000	extracted	47.7	9740	-
$\beta = 0.5$					
3	2000	20	55.6	9020	66.3
3	2000	30	50.0	9290	52.0
3	2000	50	47.0	9700	24.2
3	2000	74	47.7	9730	6.1
3	2000	150	47.7	9740	0.03
3	2000	extracted	47.7	9740	-

Table 4. Operating conditions and discharge properties for an argon ignition transient with rod position and discharge power varying simultaneously.

P [kW]	T_rod [K]	z_rod [mm]	I_coil [A/cm]	T_max [K]	$\Delta P/P$ [%]
0.5	2500	10	33.9	3410	83.3
1	2500	20	48.0	4840	84.6
1.3	2500	30	55.9	6150	83.8
1.5	2500	50	41.8	9600	39.1
1.8	2000	74	43.8	9660	12.6
2	2000	100	43.7	9690	1.4
2.5	2000	150	45.6	9720	0.02
3	-	extracted	47.7	9740	-

which would correspond to the modified conductivity (*i.e.*, $\sigma(T_\mathrm{m}^*) = \sigma(T_\mathrm{m}) + \Delta\sigma$). As the values of T_m and T_m^* suggest, the role of $\Delta\sigma$ is to make the gas behave as if it had a higher temperature, such that the corresponding value of the electric conductivity is significant.

Next, a second type of transient has been considered, in which the discharge power and the rod temperature are kept fixed while the rod is step-wise extracted. For each rod position, the time-dependent calculation has been carried out until the corresponding steady state was achieved. Simulations have been performed assuming both $\beta = 0.25\ \Omega^{-1}\ \mathrm{m}^{-1}\,\mathrm{K}^{-1}$ and $\beta = 0.5\ \Omega^{-1}\ \mathrm{m}^{-1}\,\mathrm{K}^{-1}$. The operating conditions and the discharge properties are summarized in Table 3, while the steady temperature fields for some values of the rod position are shown in Figure 8 for the case with $\beta = 0.25\ \Omega^{-1}\ \mathrm{m}^{-1}\,\mathrm{K}^{-1}$.

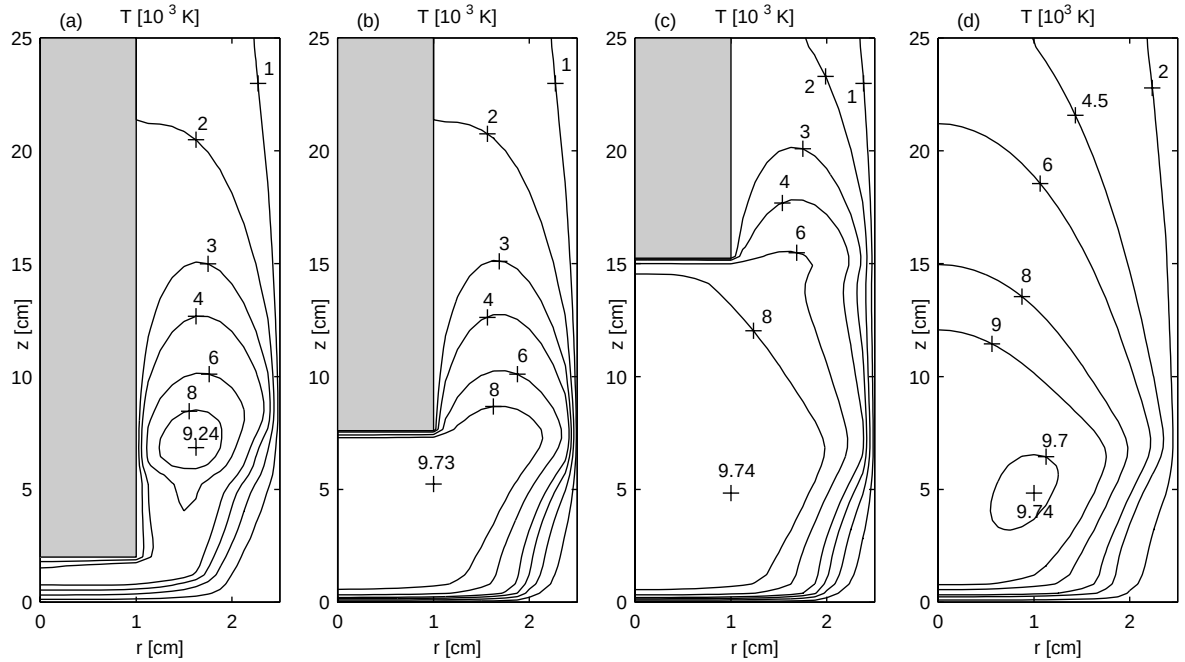

Fig. 8. Plasma temperature fields for the argon ignition transient with $\beta = 0.25\ \Omega^{-1}\ \mathrm{m}^{-1}\ \mathrm{K}^{-1}$ described in Table 3: (a) $z_{\mathrm{rod}} =$ 20 mm, (b) $z_{\mathrm{rod}} = 74$ mm, (c) $z_{\mathrm{rod}} = 150$ mm, (d) rod extracted.

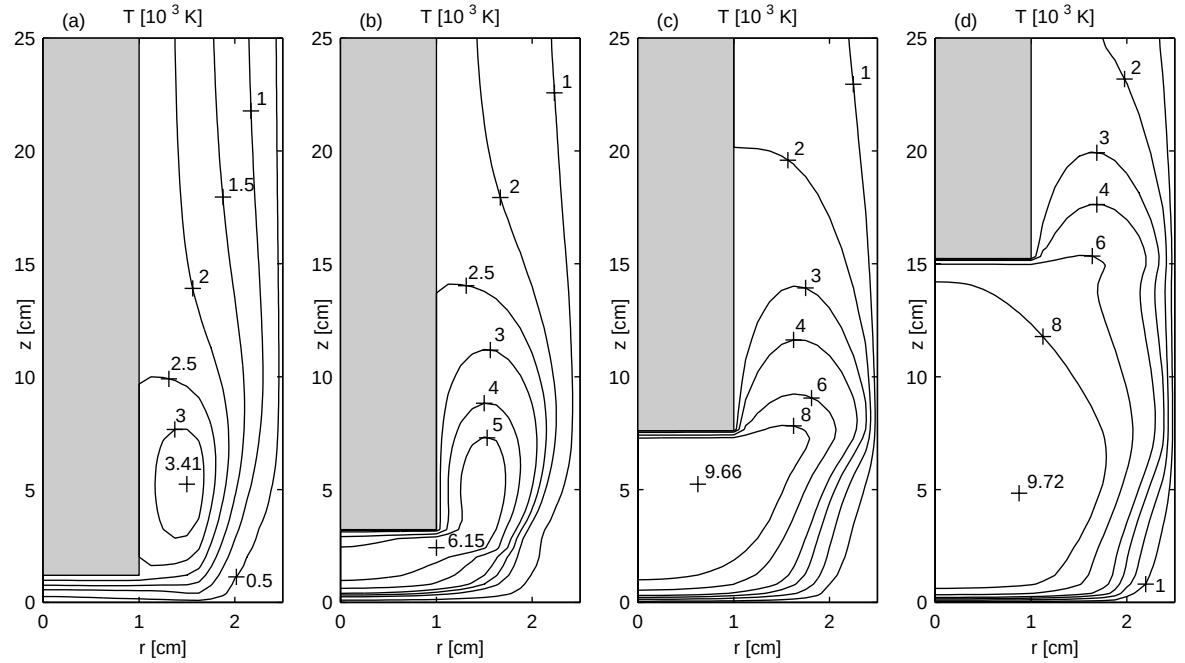

Fig. 9. Plasma temperature fields for the argon ignition transient described in Table 4: (a) $z_{\mathrm{rod}} = 10$ mm, (b) $z_{\mathrm{rod}} = 30$ mm, (c) $z_{\mathrm{rod}} = 74$ mm, (d) $z_{\mathrm{rod}} = 150$ mm. The self-sustaining configuration is the same as in Figure 8d.

A further type of ignition transient, which may be regarded as intermediate between the ones described above, has been considered. In this case, both the rod position and the power level are supposed to be varied simultaneously. For each rod position, the rod temperature is kept fixed and the corresponding steady solution is found. The detailed operating conditions and the corresponding discharge properties are shown in Table 4, while the temperature fields for some selected values of the rod position are presented in Figure 9.

Finally, a simulation of a more realistic transient describing an actual ignition procedure that could be followed in practice to obtain a steady, self-sustaining plasma discharge has been carried out. The temperature field in

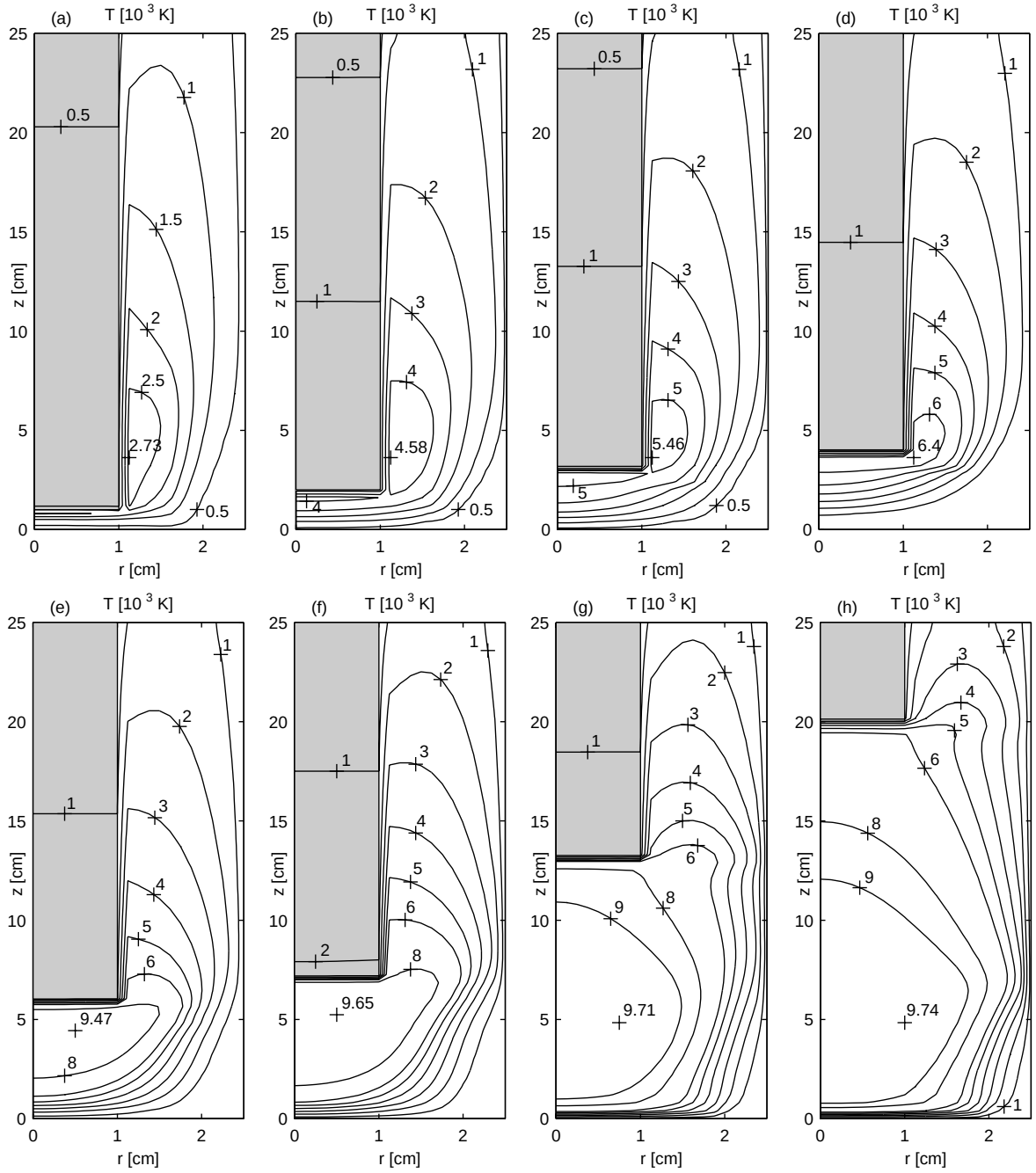

Fig. 10. Plasma temperature fields at different times for the realistic argon ignition transient described in Table 5: (a) $t = 30$ s, (b) $t = 74$ s, (c) $t = 84$ s, (d) $t = 94$ s, (e) $t = 114$ s, (f) $t = 122$ s, (g) $t = 132$ s, (h) $t = 140$ s. The self-sustaining configuration is the same as in Figure 8d.

the graphite rod has been calculated in a consistent manner with respect to the plasma temperature distribution, by solving the energy equation (4) also in the region occupied by the rod. The variation in time of the operating conditions and of the discharge properties is shown in Table 5, where T_{Ar} and T_{C} are the maximum temperatures of the gas and of the graphite, respectively, at the time t. The plasma temperature fields at different times are presented in Figure 10. For some of these cases, Figure 11 shows the plasma velocity fields. Finally, in Figure 12, plasma velocity profiles along the axis of the torch are presented for some selected values of the rod position.

4.2 Air discharges

Simulations of ignition transients for air discharges at atmospheric pressure have also been performed using the geometric and working parameters of a real torch [10]. The geometric configuration is shown in Figure 1. The working

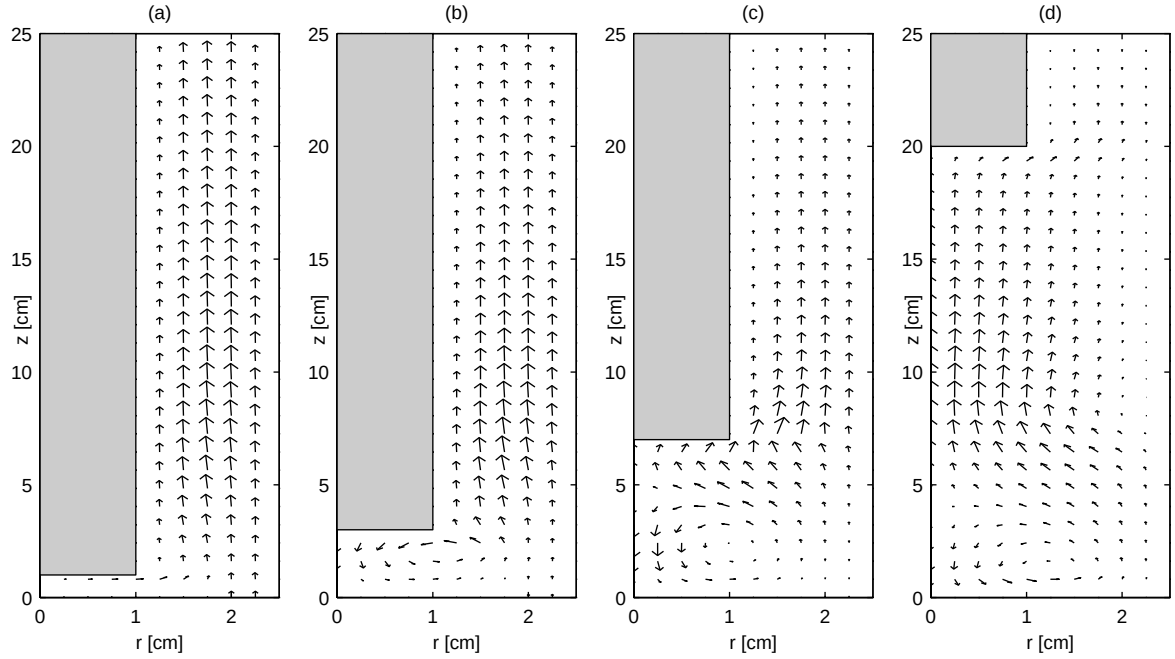

Fig. 11. Plasma velocity fields at different times for the realistic argon ignition transient described in Table 5: (a) $t = 30$ s, (b) $t = 84$ s, (c) $t = 122$ s, (d) $t = 140$ s.

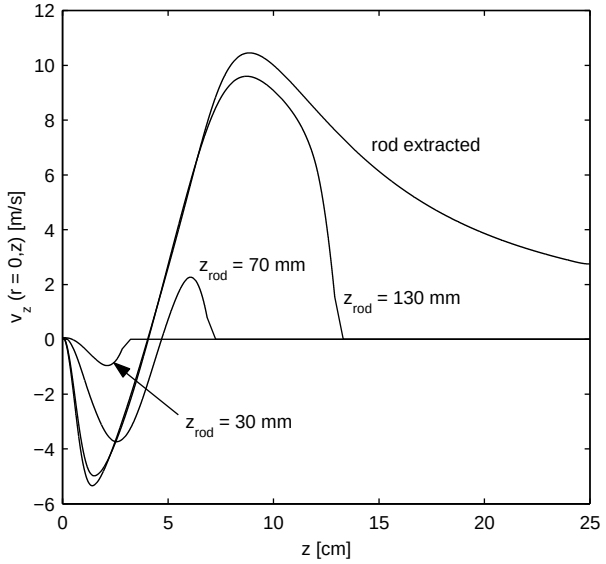

Fig. 12. Axial plasma velocity profiles for the realistic argon ignition transient described in Table 5.

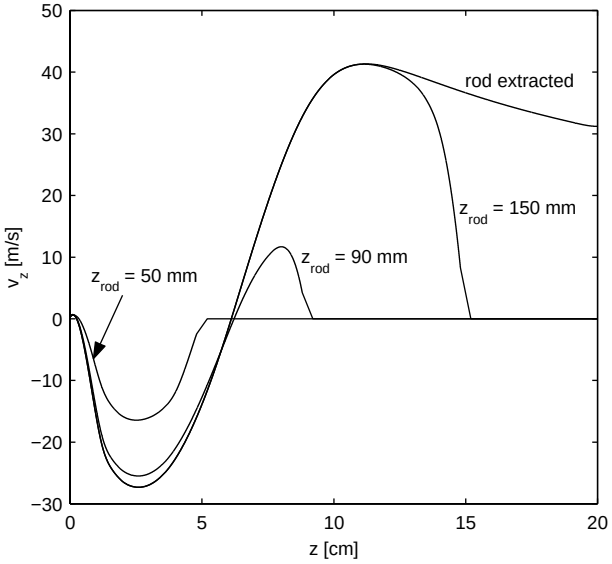

Fig. 13. Axial plasma velocity profiles for the air ignition transient described in Table 6.

conditions are: $f = 4$ MHz, $P = 27$ kW, $Q_1 = 0$ slpm, $Q_2 = 20$ slpm, $Q_3 = 100$ slpm. Results concerning a transient whose operating conditions and discharge properties are given in Table 6 are presented in Figure 13 (plasma velocity profiles along the axis of the torch) and in Figure 14 (plasma temperature fields), for different positions of the graphite rod up to the final, self-sustaining configuration. All the data shown in Table 6 refer to the steady solution corresponding to each rod position.

5 Conclusions

A two-dimensional, time-dependent, fluid magnetic code has been developed to obtain a quantitative description of the physical behaviour of inductively-coupled plasma torches during the ignition transient leading to the final, self-sustaining configuration for the plasma. The initiation technique considered makes use of a graphite rod initially inserted in the torch and then gradually extracted. The advantage of using a time-dependent code consists mainly

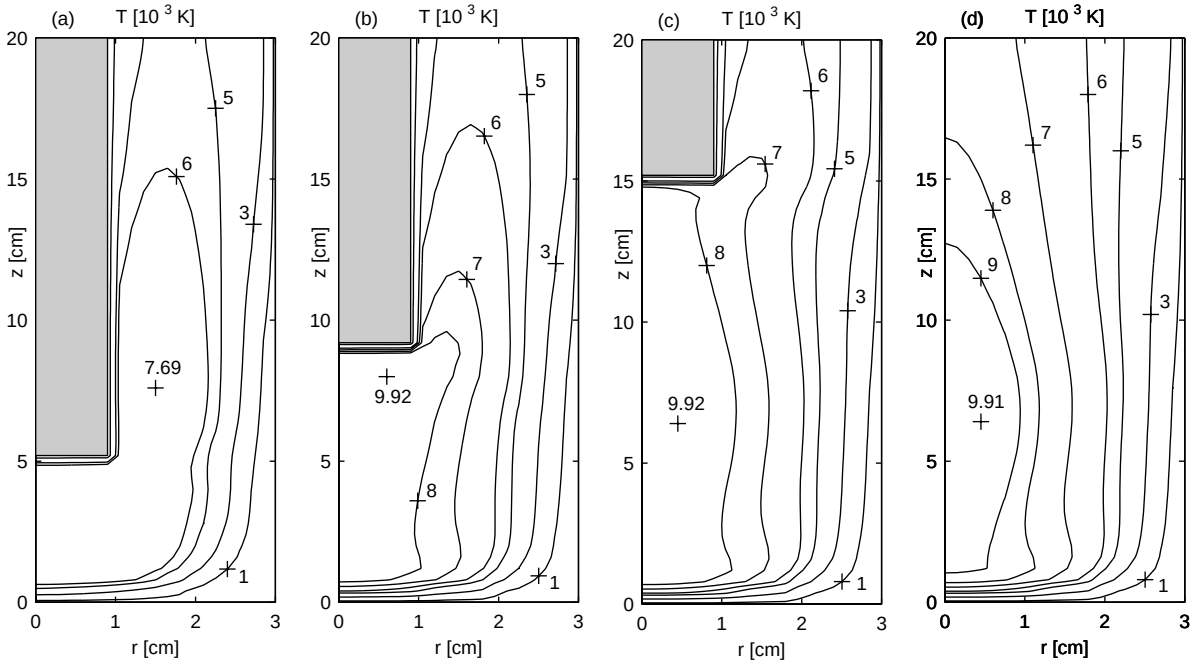

Fig. 14. Plasma temperature fields for the air ignition transient described in Table 6: (a) $z_{\rm rod} = 50$ mm, (b) $z_{\rm rod} = 90$ mm, (c) $z_{\rm rod} = 150$ mm, (d) rod extracted.

Table 5. Operating conditions and discharge properties for a realistic argon ignition transient. The calculations have been performed assuming $\beta = 0.25\ \Omega^{-1}\ {\rm m}^{-1}\,{\rm K}^{-1}$.

t	$z_{\rm rod}$	P	$T_{\rm Ar}$	$T_{\rm C}$	$I_{\rm coil}$	$\Delta P/P$
[s]	[mm]	[kW]	[K]	[K]	[A/cm]	[%]
30	10	0.3	2730	920	41.4	55.7
60	10	0.5	3890	1220	47.3	65.7
74	20	0.6	4580	1400	49.1	71.8
84	30	0.7	5460	1640	51.1	74.2
94	40	0.8	6400	1800	53.0	81.2
104	50	0.9	9110	1810	43.5	49.1
114	60	1.0	9470	1820	41.1	39.6
122	70	1.5	9650	2080	43.7	21.1
128	100	2.0	9690	1790	43.7	1.30
132	130	2.3	9710	1420	44.8	0.07
136	150	2.5	9720	1200	45.6	0.01
140	200	3.0	9740	700	47.7	0.0005
∞	extracted	3.0	9740	-	47.7	-

Table 6. Operating conditions and discharge properties for an air ignition transient. The calculations have been performed assuming $\beta = 0.25\ \Omega^{-1}\ {\rm m}^{-1}\,{\rm K}^{-1}$.

P	$T_{\rm rod}$	$z_{\rm rod}$	$I_{\rm coil}$	$T_{\rm max}$	$\Delta P/P$
[kW]	[K]	[mm]	[A/cm]	[K]	[%]
27	2000	50	124.6	7690	73.5
27	2000	90	127.3	9920	20.0
27	2000	150	126.9	9920	0.4
27	2000	extracted	126.7	9910	-

in the possibility of distinguishing between physical and numerical instabilities which occasionally may arise in the calculation. This feature is particularly attractive in the design stage of an induction torch system.

Besides, time-dependent codes permit a great flexibility in the time management of the operating conditions. Such a characteristic can be usefully exploited in order to gradually achieve working configurations for which a converged solution is difficult to obtain directly with static codes.

Moreover, the time-dependent simulation of a discharge represents a useful tool to predict the final plasma temperature and velocity fields for some types of non-conventional torch configurations. In particular, time-dependent simulations are very helpful in the study of RF-RF hybrid torches [11,12], where the presence of multiple self-sustaining equilibrium configurations corresponding to the same operating conditions may cause the failure of the numerical procedure when using static analyses.

This work has been performed with the partial financial support by the Association for the Scientific and Technological Development of Piemonte (A.S.S.T.P.), Torino, Italy.

References

1. M.I. Boulos, Pure Appl. Chem. **57**, 1321 (1985).
2. J. Mostaghimi, P. Proulx, M.I. Boulos, Plasma Chem. Plasma Process. **4**, 199 (1984).
3. Xi Chen, E. Pfender, Plasma Chem. Plasma Process. **11**, 103 (1991).

4. J. Mostaghimi, M.I. Boulos, Plasma Chem. Plasma Process. **9**, 25 (1989).
5. V. Colombo, C. Panciatichi, A. Zazo, G. Cocito, L. Cognolato, IEEE Trans. Plasma Sci. **25**, 1073 (1997).
6. Xi Chen, J. Phys. D: Appl. Phys. **22**, 361 (1989).
7. S. V. Patankar, *Numerical Heat Transfer and Fluid Flow* (Hemisphere Publishing Corporation, New York, 1980).
8. R.C. Miller, R.J. Ayen, J. Appl. Phys. **40**, 5260 (1969).
9. M. Capitelli, G. Colonna, C. Gorse, A. D'Angola, Eur. Phys. J. D **11**, 279 (2000).
10. Y.P. Raizer, *Gas Discharge Physics* (Springer-Verlag, Berlin, Heidelberg, 1991), p. 317.
11. D. Bernardi, V. Colombo, G.G.M. Coppa, E. Ghedini, A. Mentrelli, Investigation on Operating Conditions and Efficiency Optimization of RF-RF Hybrid Plasma Torches, in press on *Advances in Thermal Plasma Processing, Begell House Inc., Proceedings of the 6th International Thermal Plasma Processing Conference*, Strasbourg (France), May 30-June 2, 2000.
12. D. Bernardi, V. Colombo, G.G.M. Coppa, E. Ghedini, A. Mentrelli, Numerical Modelling of RF-RF Hybrid Plasma Torches and Parametric Study for Various Geometric, Flow and Electric Configurations, in press on *Advances in Thermal Plasma Processing, Begell House Inc., Proceedings of the 6th International Thermal Plasma Processing Conference*, Strasbourg (France), May 30-June 2, 2000.